Han, Y., Noah, M., Lüders, V., Horsfield, B., Mangelsdorf, K. (2020): NSO-compounds in oil-bearing fluid inclusions revealed by FT-ICR-MS in APPI (+) and ESI (−) modes: A new method development. - Organic Geochemistry, 149, 104113.

https://doi.org/10.1016/j.orggeochem.2020.104113

NSO-compounds in oil-bearing fluid inclusions revealed by FT-ICR-MS in APPI (+) and ESI (-) modes: A new method development

Yufu Han[a,*], Mareike Noah[a], Volker Lüders[a], Brian Horsfield[b], Kai Mangelsdorf[a]

[a]Helmholtz Centre Potsdam GFZ - German Research Centre for Geosciences, Department of Geochemistry, Section 3.2 Organic Geochemistry, Telegrafenberg, Potsdam, Germany;

[b]GEOS4 GmbH, D-14552 Michendorf, Germany

* Corresponding author: Email address: yhan@gfz-potsdam.de,

Tel: +49 33128828688

Abstract: The origins of hydrocarbons occurring in oil-bearing fluid inclusions (FIs) have been studied in detail over the last four decades, but very little is known about co-occurring nitrogen, sulfur and oxygen (NSO)-containing compounds. Here, we outline a new method for gathering valuable information on NSO compounds using the Fourier Transform-Ion Cyclotron Resonance-Mass Spectrometry (FT-ICR-MS) in combination with Atmospheric Pressure Photoionization in positive ion mode (APPI (+)) and Electrospray Ionization in negative ion mode (ESI (-)). A key element was to develop a rigorous acid-free cleaning protocol to make oil inclusions from a broad range of host materials accessible to the very sensitive FT-ICR-MS technique. Although oil contamination from surrounding organic matter can never be entirely eliminated, the procedure enables distinction of external contaminants and identification of affected NSO compound classes allowing a conditional interpretation

of the FT-results of FI samples, especially for compounds measured in the APPI (+) mode. First insights into the high molecular weight hydrocarbons and NSO-compounds in fluid inclusion oils are presented here using examples from Germany, Tunisia, Pakistan and Mexico.

Keywords: NSO-compounds; oil-bearing fluid inclusions; clean-up method; FT-ICR-MS

1. Introduction

Oil-bearing fluid inclusions (FIs) hosted in minerals such as e.g., fluorite, quartz or carbonates contain aliquots of oil that were trapped within cavities during crystal growth as primary FIs or during re-crystallization of secondary cracks in the presence of a fluid phase (e.g., Burruss, 1981; Roedder, 1984; Goldstein, 1994; Munz, 2001). In general, petroleum FIs are trapped in cements, and/or fracture-fill mineralization hosted by sedimentary rocks. Abundant oil-bearing FIs are reported from sediment-hosted Mississippi Valley-type (MVT) deposits, where they are typically contained in fluorite, but also in barite, carbonate and/or sphalerite (Etminan and Hoffmann, 1989; Guilhaumou et al., 2000; Benchilla et al., 2003; González-Partida et al., 2003). The geochemical information received from the analysis of FIs oils has been used to compare present and paleo-oils (early oil charges) and to examine migration events and alteration processes that have affected the composition of the oil (Horsfield and McLimans, 1984; Bodnar, 1990; Lisk et al., 1996; George et al., 1997, 2004; Volk and George, 2019). The great advantage of using FI oils is that the oil is

physically isolated from the main pore system of the reservoir rock, and therefore events affecting the reservoir such as leakage, water-washing, biodegradation and contamination associated with drilling do not affect the composition of the inclusion oil. Comprehensive reviews of FI oils and applications have been published by George et al. (2007) and Volk and George (2019).

The composition of fluids in oil FIs is complex, with components including gases (such as CH_4, CO_2 and N_2), higher molecular weight hydrocarbons (aliphatic and alkylaromatic), NSO-compounds (containing nitrogen, sulfur and/or oxygen as heteroatoms), and water (Roedder, 1984; Pang et al., 1998; Burruss, 2003). Murray (1957) was the first to unravel the composition of FIs-occluded oils, employing mass spectrometry to analyze light hydrocarbons and gases. Since then many different analyses have been applied to unravel the bulk composition of included oils, such as gas chromatography with a flame ionization detector (GC-FID) (Horsfield and McLimans, 1984), gas chromatography-mass spectrometry (GC-MS) (Karlsen et al., 1993; George et al., 1997), and high performance liquid chromatography (HPLC) (Pang et al., 1998). Techniques for analyzing individual oil inclusions also have been developed, such as time-of-flight secondary ion mass spectrometry (ToF-SIMS) using an ion gun (Siljeström et al., 2010, 2013), GC-MS with an on-line femtosecond laser (Volk et al., 2010), and GC-MS with an on-line excimer laser (Zhang et al., 2012). Aliphatic, aromatic and tetra- and pentacyclic hydrocarbons as well as low molecular weight NSO-compounds, such as phenols and carbazoles (Ruble et al., 1998; George et al., 2004; Peters et al., 2018) were the main target classes under study.

As compared to crude oils, inclusion oils are preferentially enriched in polar compounds (Karlsen et al., 1993; Nedkvitne et al., 1993), because they are more readily adsorbed on mineral surfaces during inclusion formation (Crocker and Marchin, 1988; Pang et al., 1998; George et al., 2007). Yet, very little compositional insight has to date been gathered on high molecular weight NSO-compounds in FI oils. Here, we utilize the Fourier Transform-Ion Cyclotron Resonance-Mass Spectrometer (FT-ICR-MS) with its ultra-high mass accuracy to study NSO-compounds in FI oils, identifying molecular formulae and resolving thousands of compounds that are inaccessible to GC-FID and GC-MS (Marshall and Rodgers, 2004, 2008). Many geological questions have been addressed using this instrument recently, such as organic matter maturation (Hughey et al., 2004; Oldenburg et al., 2014; Poetz et al., 2014), biodegradation (Huang et al., 2003, 2007; Kim et al., 2005; Liao et al., 2012; Seidel et al., 2016; Martins et al., 2017; Oldenburg et al., 2017), oil migration (Oldenburg et al., 2014; Liu et al., 2015; Han et al., 2018; Ziegs et al., 2018), as well as oil and source rock correlation (Mahlstedt et al., 2016). Thus, this powerful instrument also could offer a new approach to shed light on polar compounds trapped in FI oils.

The indigenous organic matter surrounding FIs, and contaminants from drilling and sampling adhering on the surface or in microcracks of host minerals, may affect inclusion oil analysis. In previous studies, strong acids such as hydrochloric acid and chromic acid were applied to clean host minerals (George et al., 2007). However, this method is clearly unsuitable for carbonate minerals. For carbonate rocks various

organic solvents, like dichloromethane and other solvent mixtures, have been used to repetitively wash host minerals using Soxhlet, sonication extraction or vacuum solvent extraction (Karlsen et al., 1993; George et al., 1998, 2007; Jones and Macleod, 2000). Such clean-up procedures have successfully been used prior to the GC-MS analysis of FI oils (Jones and Macleod, 2000; Volk et al., 2002; George et al., 2007). Noah et al. (2018, 2019) were the first to demonstrate that FT-ICR-MS can be used to analyze NSO compounds in fluid inclusion oils contained in quartz, applying the clean-up methods developed by George et al. (2007). Noah et al., (2018; 2019) compared FT-ICR-MS derived NSO compound compositions in a FI oil, a produced oil, potential source rock extracts and reservoir rock extracts from the Üllés Field in the Pannonian Basin, Hungary. They found elevated abundances of NSO compounds in FI oils compared to crude oils, which may reflect the greater affinity of NSO compounds to polar mineral surfaces, where oils can be trapped on crystal imperfections. Furthermore, they demonstrate that FT-ICR-MS can be used as a tool to provide detailed information on NSO compounds in FI oils. First high resolution mass spectrometry results showed systematic variations in NSO compound composition between sample types. This opened an exciting domain of research into mineral-fluid interaction and the evolution of petroleum reservoirs.

First extraction experiments in our study showed that the conventional cleaning methods developed for GC-MS not always provide the level of purity needed for the very sensitive FT-ICR-MS technique and that additional cleaning steps are needed. Furthermore, conventional methods often use strong acids and cannot be applied to

host crystals that react with acids, namely fluorite and carbonates.

Thus, in this study an acid-free clean-up and preparation procedure is presented that is suitable for all host mineralogies. It eliminates organic contaminants adhering to host mineral surfaces and thereby enables polar compounds in FI oils to be analyzed using FT-ICR-MS in APPI (+) and ESI (-) ionization modes. These ionization modes were selected because they are the most common in crude oil characterisation and because they provide the broadest range of compound polarities and ionization efficiencies. Four representative samples with microscopically characterised oil-inclusions in different host minerals have been chosen for the method development to characterise occluded NSO-compounds in FI oils.

2. Material and Methods

2.1. Sample set and geological background

Oil can be trapped in fluid inclusions hosted in different minerals which were formed in various sedimentary settings (Roedder, 1984). For example, fracture-fill mineralization may contain abundant FIs that contain instantaneously generated oil (Roedder, 1984; Etminan and Hoffmann, 1989; Benchilla et al., 2003). The samples studied here originated from two MVT-type deposits in Tunisia and Mexico and consist of fluorite. In addition, quartz samples from two occurrences, namely quartz veins hosted by Triassic sandstones from Germany and vugs from an ore deposit in Pakistan were studied (Fig. 1). Detailed geological information on each sample is provided in Table 1.

132

133 *2.1.1 Quartz sample from Germany*

134 Colorless quartz from veins hosted in an Upper Triassic sandstone from the
135 Lower Saxony Basin (LSB) located in north-western Germany hosts abundant oil and
136 gas-bearing inclusions. The oil inclusions show liquid-vapor (L-V) homogenization at
137 mean temperatures of 137.1 °C (Fig. 1a). The formation of quartz was triggered by
138 fluid migration in response to tectonic movements of the LSB. A period of rifting and
139 wrench tectonics occurred during the Late Jurassic and Early Cretaceous (Betz et al.,
140 1987). During this period oil migrated and was preserved as FIs in quartz fracture-fill
141 mineralization. The oil trapped in quartz was considered to be sourced from Lower
142 Jurassic Posidonia shale (Lüders et al., 2012) which is the most important source rock
143 for oil (and gas) in the LSB (Lüders and Plessen, 2015 and references therein).

144

145 *2.1.2 Fluorite sample from Tunisia*

146 The Tunisian fluorite sample is colorless and hosts large oil fluid inclusions with
147 sizes up to 400 μm (Fig. 1b). The fluorite mineralization in north-eastern Tunisia
148 occurs along the Zaghouan and Hammam Jedidi faults, which have been tectonically
149 active since the Late Miocene (Bouhlel et al., 1988). In the Late Tortonian-Pliocene,
150 petroleum that was generated from Triassic-Permian sediments migrated with
151 hydrothermal brines into the Campanian series and Tithonian series limestones in
152 Hamman Zriba (Benchilla et al., 2003). The mineral association is similar to
153 MVT-type deposits (Cathles and Smith, 1983). Bouhlel et al. (1988), distinguished

between three styles of fluorite mineralization in this area: white vein-type fluorite (F1 type), massive purple fluorite (F2 type) and massive white fluorite in cavities and open vugs (F3 type). All fluorite types contain abundant oil-rich FIs. In the current study, a F3 fluorite sample was investigated. Homogenization temperatures of petroleum FIs vary between 173 °C - 194 °C ± 10 °C and salinities between 13 to 22% (Guilhaumou et al., 2000; Benchilla et al., 2003).

2.1.3 Quartz sample from Pakistan

The quartz crystals from Pakistan exhibit prominent prismatic or steep rhombohedral habits with dark material trapped inside (Fig. 1c). L-V homogenization of oil-bearing FIs in the temperature range between 121.8 and 162.8 °C was measured. Oil-bearing FIs hosted in fluorite and quartz were reported in the Koh-i-Maran region (Pakistan) (Benchilla et al., 2003). In the early Oligocene, oil generated from Lower Jurassic sediments and migrated with brines into the Upper Jurassic limestones. Bipyramidale quartz crystals from the Koh-i-Maran region resemble the well-known "Herkimer diamonds" (Ulrich, 1989).

2.1.4 Fluorite sample from Mexico

The purple fluorite sample from Encantada-Buenavista, Mexico is prone to crack along its cleavage and has an intense petroleum odour after cracking (Fig. 1d). During the Tertiary, oil and aqueous fluids penetrated a network of fractures in Upper Cretaceous shales and carbonates resulting in the precipitation of fluorites rich in oil

FIs. Fluorite mineralization was similar to those described for Tunisia and other MVT-type deposits. L-V homogenization temperatures of FIs hosted in fluorite were documented between 139.6 and 153.2 °C. Oil was considered to have been sourced from calcareous shale and carbonates of the Upper Jurassic and to a lesser extent by Tertiary and Cretaceous rocks (González-Partida et al., 2002, 2003).

2.2 Host mineral clean-up

For the clean-up procedure high-purity solvent and clean glassware were utilised. High-purity dichloromethane and methanol (99.9% hypergrade for LC-MC), sodium dithionite ($Na_2S_2O_4$), sodium bicarbonate ($NaHCO_3$) and sodium citrate ($Na_3C_6H_5O_7$) (>99% grade) were used. Extraction thimbles were ultrasonically pre-cleaned for 30 minutes using dichloromethane as solvent, followed by Soxhlet extraction with dichloromethane for 24 hours. Glassware was cleaned using a commercial surfactant solution (Neodisher LabClean FLA), then heated to 450 °C in an oven and finally rinsed three times with DCM before utilization.

In the first clean-up step minerals were coarsely broken with a hammer, splitting along cracks and fractures, and the mineral fragments were washed using distilled water and then dried. Afterwards, a Waller solution (33% sodium dithionite, 28% sodium bicarbonate, 59% sodium citrate in distilled water) (Nichols, 2019) was added to oxidize iron and organic matter on the surface of the host mineral fragments. While the oxidizing ability of the Waller solution is weaker than the commonly applied chromic acid, it is from a safety aspect less harmful and, of paramount importance,

198 suitable for carbonate mineral clean-up. The host minerals were kept in the Waller
199 solution for 3 hours followed by a sonication for 10 min. Subsequently, the mineral
200 material was washed twice using distilled water and dried. This step was repeated
201 three times.

202 In the second step, a modified multiple cleaning procedure was established based
203 on the protocol of George et al. (2007). The minerals were washed in sequence with
204 solvents or solvent mixtures with decreasing polarity. The host minerals were cleaned
205 with 30 mL of methanol, followed by 30 mL of a mixture of dichloromethane (DCM)
206 and methanol (93:7, v/v) and finally by 30 mL of DCM using ultrasonication for 10
207 minutes each time. Each washing step was conducted three times.

208 After these rigorous cleaning procedures the final washing step with DCM was
209 collected as a blank for conventional GC-MS analysis. However, it turned out that this
210 blank was not suitable for FT-ICR-MS analysis, since it still contained some tiny
211 mineral particles which were prone to block the transfer capillary (capillary for ion
212 transfer from the ion source (ambient pressure) into the MS with high vacuum
213 conditions) of the FT-ICR-MS. Thus, the solvent cleaned host minerals were
214 transferred into an extraction thimble within a Soxhlet apparatus and washed twice for
215 24 h with 250 mL DCM and methanol (99:1, v/v) at 50 °C. The solvent of the final
216 washing step was collected, concentrated by a Turbovap system (Biotage) and dried
217 under a N_2 stream. This clean-up solution is used as the procedural blank (P-blank).
218 Before measuring any sample, pure solvent was measured on the FT-ICR-MS system
219 to obtain a system blank (S-blank) for comparison.

220

221 *2.3 Extraction of inclusion oils*

222 Cleaned host minerals were loaded into a crushing cylinder equipped with two
223 stainless steel balls. The host minerals were crushed by shaking, after which the
224 crushing cylinder remained stationary for 10 min. The mineral powder was transferred
225 into pre-cleaned extraction thimbles. The steel balls and crushing cylinder were rinsed
226 by DCM and methanol (99:1, v/v) and the washings were added to the Soxhlet
227 thimble. Afterwards, the mineral powder was extracted by Soxhlet extraction for 24 h
228 with 250 mL DCM and methanol (99:1, v/v) at 50 °C. Finally, the Soxhlet extract was
229 concentrated by a Turbovap system and dried under a stream of N_2. The extracted FI
230 oil was weighed and measured by FT-ICR-MS in both APPI (+) and ESI (-) modes.

231

232 *2.4 Analytical methods*

233 *2.4.1 Microscopy*

234 Doubly polished thin sections of the minerals were used to observe the oil FIs
235 using a BX50 Olympus microscope with various objectives (5×, 10×, 20×, 50×)
236 connected to a UV light device.

237 *2.4.2 FT-ICR-MS measurement*

238 Blanks and inclusion oils were measured using a 12T Solarix FT-ICR-MS from
239 Bruker Daltonik GmbH (Bremen, Germany) in ESI (-) and APPI (+) ionization mode.
240 A detailed description of the equipment, mass calibration and data analysis for ESI (-)
241 mode has been presented by Poetz et al. (2014). For ESI (-) mode, a stock solution of

1 mg/mL in methanol and toluene (1:1, v/v) was diluted with the same solvent mixture to give a final concentration of 100 μg/mL. Before analysis, 1 mL sample solution was mixed with 10 μL of a 25% aqueous NH_3 solution to facilitate the deprotonation of the molecules for analysis. The working parameters were as follows: nitrogen flow rate 4.0 L/min, temperature at 220 ℃, nebulizing gas 1.4 bar, sample solution flow rate 150 μL/h, capillary voltage 3000 V, additional collision-induced dissociation voltage of 70 V, ions accumulation time 0.05 s, transfer time 1 ms, 4 megaword data sets. A total of 200 mass spectra were accumulated in a mass range from *m*/*z* 147 to 1000. External calibration for ESI (-) mode was performed using an in-house fatty acid and polyethylene glycol sulfate mixture.

For measurements in APPI (+) mode, a concentration of 1 mg/mL in methanol and hexane (9:1, v/v) was diluted with the same solvent mixture to give a final concentration of 20 μg/mL. The working parameters were as follows: dry gas (N_2) flow rate 3.0 L/min and temperature 210 °C, nebulizing gas (N_2) 2.3 bar, sample solution flow rate 20 μL/h, capillary voltage 1000 V, additional collision-induced dissociation voltage of 30 V, ions accumulation time 0.03 s, transfer time 1 ms, 4 megaword data sets. A total of 300 mass spectra were accumulated in a mass range from *m*/*z* 147 to 1200. External calibration for the APPI (+) mode was done using a calibration mixture containing polyethylene glycol 400 and polyethylene glycol 600 (1:1) from Fluka.

In each spectrum, signals with a signal-to-noise ratio ≥ 12 were included into the further data assessment. Formula assignment was done using the isotopes ^{1}H, ^{12}C, ^{13}C,

^{14}N, ^{16}O, and ^{32}S, with the upper thresholds N ≤ 2, O ≤ 8, and S ≤ 2 in APPI (+) mode and N ≤ 2, O ≤ 8 and S = 1 in ESI (-) mode; C and H were unlimited. If no chemical formula within the allowed mass error of 0.5 ppm was found, the peak was not included into the mass/formula list. For each $C_cH_hN_nO_oS_s$ compound, its double bond equivalent (DBE) value was obtained by calculating DBE=c-h/2+n/2+1. Each DBE refers to the number of unsaturation or rings in the individual compound structure.

2.4.3 GC-MS measurement

FI oils were analyzed by GC-MS after FT-ICR-MS. Prior to GC-MS analysis 5α-Androstane and 1-ethylpyrene were added as internal standards. The FI oils were analyzed using a Trace GC Ultra coupled to a DSQ mass spectrometer (Thermo Electron Corp.). The GC was equipped with a Thermo PTV injection system and a SGE BPX5 fused silica capillary column (50 m × 0.22 mm ID and 0.25 μm film thickness). Helium was used as carrier gas. Samples were heated in the GC oven from 50 °C to 310 °C at a rate of 3 °C/min, and held at the end temperature for a further 30 minutes. The injector temperature was programmed from 50 °C to 300 °C at a rate of 10°C/s. The MS was operated in electron impact ionization mode (EI) at 70 eV. Full-scan mass spectra were recorded from m/z 50-600 at a scan rate of 1.5 scans/s.

3. Results and discussion

3.1 Microscopic characterization of fluid inclusions

FI oil characteristics were studied using both transmitted and UV light (Fig. 2). The oil inclusions in fluorite samples TN and MX are pale yellow under transmitted light, making it easy to distinguish them from co-genetically trapped colorless aqueous FIs. In contrast, the inclusion oils in the quartz samples GE and PK were colorless (Fig. 2). Oil inclusions in samples GE and MX range from 10 to 50 μm, and were more abundant in the MX sample than in the GE sample. Globular oil inclusions were common in the TN sample with diameters up to 400 μm. Oil inclusions in the PK sample showed variable shapes, reaching several hundred micrometers in size and containing large vapor bubbles. Several examples of solid bitumen trapped in inclusions were documented (Fig. 2c) in the PK sample which may have formed during the transformation of oil to gas at high temperature (Burruss, 2003). Most oil FIs consisted of either gas and liquid (either oil or water), or three phases (gas, liquid and solid bitumen). It has generally been demonstrated that blue and white fluorescence of inclusion oils indicate higher maturity (Burruss et al., 1985; McLimans, 1987). Oil FIs in samples GE, TN, and PK were deep blue, pale blue and light blue, respectively, under UV light, while they were nearly white in sample MX. The blue to white fluorescence points to low density of the oil inclusions, reflecting high API gravity (Burruss, 2003). It is assumed that the oil trapped in inclusions was generated from a source rock whose maturity was ca. 0.93% (TN), 1.31% (PK), and 0.97% (MX), as estimated using MPI-1 ratios (Table 2). An R_o value of about 0.78% for the GE sample (Table 2) was calculated on the base of carbon isotope ratio of oil-bearing fluid inclusions by Lüders et al. (2012).

3.2 Extraction yields

The amounts of oils extracted from FI varied between 0.38 mg and 3.12 mg (Table 2). This resulted in extraction yields of 56 to 366 µg/g host mineral. The PK quartz sample showed the highest and the GE fluorite sample the lowest extraction yield, while the MX fluorite and TN quartz samples showed intermediate concentrations.

3.3 Contaminant assessment in fluid inclusion oils

The extracted oils, system blanks (S) and procedural blanks (P) were analyzed by FT-ICR-MS in the APPI (+) and ESI (-) modes. For the interpretation of the FT-ICR-MS data of the extracted FI oils it is especially important to identify indigenous signals and distinguish them from external sources. This is especially important because the occluded oils are present in low concentration. To assess the level of external components in the FI oil extracts, all signals detected were compared to the signals occurring in the S-blank and P-blank samples applying a Venn analysis (Oliveros, 2007) (Fig. 3). With this method, both unique and common signals from the different samples were revealed. Due to the ultrahigh resolution and sensitivity of the FT-ICR-MS organic compounds were detected even in the S-blank representing a measurement of a hypergrade solvent. However, the number of components common to the S-blank and the inclusion oils was small (0 to 19 signals) for both ionization modes, while the number of shared signals with all sample types were more abundant

330 (68 to 229 signals). This most likely represented background signals of the
331 measurement system. In contrast, the number of common signals between the FI oils
332 and the P-blanks was significantly higher (101 to 504 signals). This might represent
333 compounds still adhering on the mineral matrix even after the stringent clean-up
334 procedure. On the other hand, it can also be argued that these signals also contained
335 compounds which were present on the mineral surfaces as well as in the FI oils.
336 However, there is no way to separate this and thus, to be on the safe side, these shared
337 compounds were assessed as contaminants for the FI oils. Although there was a
338 certain number of shared compounds between the P-blank and FI oil samples, in both
339 ionization modes the number of unique compounds was in most cases highest for the
340 extracted oils. One exception was given by the GE sample in the APPI (+) mode. The
341 reason for this might be that this is the sample with the lowest extraction yields (Table
342 2).

343 Thus the Venn diagram proved to be valuable providing a first assessment of the
344 level of external contamination of the FI oils and to check how well the cleaning
345 procedure had worked. On first inspection the comparison of all assigned signals
346 presented in Figure 3 suggests a successful cleanup for the processed FI samples.

347 For a deeper assessment as to which compounds and compound classes can be
348 used for further data interpretation, it is necessary to compare each compound class
349 and its DBE distributions in the inclusion oils with those from the blanks. According
350 to this comparison there were three different assessment categories defined: The
351 assessment category I (high contamination level) is exemplified by the O_4 class in the

GE sample measured in APPI (+) mode (Fig. 4). The comparison shows a very similar compound distribution for the extracted inclusion oil and both the S- and P-blanks, (Fig. 4a). Therefore, these compounds might have been introduced into the FI oil extract by contaminants still adhering on the mineral surface (P-blank) and/or by the solvent or measurement procedure (S-blank). These compound classes do not give reliable information on the oil and can be assessed as contamination.

Category II (low contamination level) was represented for instance by the HC species in the TN sample measure in the APPI (+) mode showing also a few distinct compounds (red square in Fig. 4b) which were present in both blanks and the FI oil, but additionally a high number of HC compounds which were unique to the oil. Here only a selected part of the HC compounds was assessed as being contaminants, while the overwhelming remaining majority were considered as indigenous for the FI oil.

Category III (non-contamination level) was illustrated by the N_1 compound class from the MX sample measured in the ESI (-) mode. The corresponding S- and P-blanks were completely free from N_1 compounds, indicating that the only source of these compounds is the FI oil itself (Fig. 4c).

In accordance with these three categories, the main compound classes were fully suitable or conditionally suitable (categories III and II, respectively) or unsuitable (category I) for further interpretation (Table 3). Thus, although contributions from external contamination sources cannot completely be avoided, the presented method shows that the level of contamination can be assessed and that the affected compound classes can be identified, thus enabling FI signals to be recognized. Figure 5a

374 indicates that the dominant compound classes in APPI mode show no or only a low
375 level of contamination (compare with Table 3). By contrast, in ESI (-) mode, only
376 selected compound classes show an acceptable level of contaminants. Thus, although
377 the Venn diagrams (Fig. 3) suggested a similar contamination level for the two
378 ionization modes, the detailed compound class analysis (Table 3) indicates that the
379 clean-up procedure worked much better for the compounds which can be measured in
380 APPI (+) mode. A reason for this could be that compounds which are measurable in
381 the ESI (-) mode usually show a much higher polarity and therefore adhere much
382 better on mineral surfaces (Marshall and Rodgers, 2008). However, the Pakistan
383 sample shows acceptable levels of contamination for almost all compound classes,
384 (Table 3) and also the Mexican sample indicates for the dominating O_2 and N-classes
385 that the clean-up procedures can partly be sufficient also for the ESI (-) mode. It is not
386 very likely that this different behavior is dependent on the mineral matrix, since one
387 quartz sample show massive contamination (GE) and the other not (PK). It is
388 conceivable that the amount of extractable FI oil plays a more significant role for the
389 compounds measurable in the ESI (-) mode. The amount of the GE and TN sample is
390 significantly lower than for the MX and especially for the PK sample (Table 2), thus
391 acidic contaminants, which are also common in the laboratory environments, have a
392 much higher impact on the GE and TN samples. To conclude, the data suggest that
393 only FI samples with a high extraction yield should be analyzed in the ESI (-) mode or
394 that an even more intensive cleaning method is needed for the ESI (-) mode to reduce
395 external contamination to an acceptable level. Nevertheless, considering the presented

contamination assessment the presented method enables access to the NSO compound fraction from FI oils allowing the investigation of their geochemical significance.

3.4 NSO-compounds and hydrocarbons in inclusion oils as geochemical markers

In the following examples we demonstrate how compounds or compound classes from FI oils, assessed as suitable (category III) and conditionally suitable (category II) for further interpretation, can be applied to address various petroleum geological issues, namely intitial petroleum compositions, thermal maturity and biodegradation levels.

3.4.1 Characteristic compositions of inclusion oils

Fluid inclusion oil analysis can provide deep insights into the original oil composition which becomes especially important when reservoir oil is altered by subsequent processes. Figure 5a shows the distribution of low polarity NSO-compounds and aromatic hydrocarbons detected in the four investigated FI oils using the APPI (+) mode. Comparing Figure 5a with Table 3 it becomes clear that the dominating compound classes (HC, O_1, O_2 and S_1) are not significantly affected by external contamination and that these groups can be used for further oil characterization and interpretation. In contrast, the higher abundance of the O_4 compounds in the GE and TN samples might reflect external contamination. Overall, the compound inventory of the investigated FI oils showed a broad variability from pure hydrocarbons (HC) to compounds with different numbers and combinations of hetero-atoms (Fig. 5a) and differences between the investigated FI oils can clearly be

418 recognized.

419 In the ESI (-) mode the acidic NSO compounds are detected. Thus, the
420 compound class distribution in all samples (Fig. 5b) was dominated by
421 oxygen-containing compounds, especially by O_2, O_3 and O_4 species. The N_1 species
422 are major contributing classes as well. As discussed above in the ESI (-) mode
423 residual contamination is a greater issue than in the APPI (+) mode. However, the
424 level of contamination also seems to depend on individual sample characteristics and
425 extraction yields of FI oils, since the PK FI oil shows only low and acceptable
426 contamination levels, while the TN sample can essentially not be evaluated. However,
427 with the exception of the TN sample the main compound class (O_2 class) can be used
428 for further interpretation. The same is true for the N_1 class and for S_1O_1 species at
429 least for the TN, PK and MX FI oils.

430

431 *3.4.2 Thermal maturity assessed from inclusion oils*

432 NSO-compound parameters that have been employed for assessing thermal
433 maturity have been discussed in many studies based on nitrogen and sulfur-containing
434 compounds from reservoir petroleum. N_1 compounds, especially pyrrolic nitrogen,
435 have been widely studied using the ESI (-) mode and relationships between N_1
436 compound compositions and thermal maturity have been established (Hughey et al.,
437 2004; Oldenburg et al., 2014; Poetz et al., 2014; Mahlstedt et al., 2016). The same is
438 true for S_1 compounds which have been studied in APPI (+) mode (Oldenburg et al.,
439 2014; Walters et al., 2015) and ESI (+) mode (Li et al., 2011). In addition to the polar

compounds thermal maturity is also expressed in compositional changes of aromatic hydrocarbons detected in the APPI (+) mode (Purcell et al., 2006; Rodgers and Marshall, 2007), since thermal maturation promotes aromatization of the organic matter (Tissot and Welte, 1984).

Maturity assessment using nitrogen-containing compounds in inclusion oils

N_1 compounds were highly abundant in the MX FI oil, with DBE in the range from 9 to 21, and carbon numbers ranging from 19 to 42 (Fig. 4c). DBE 12 and 15 classes were preferentially enriched, and these compounds could be interpreted as consisting of a carbazole unit and additional benzene rings, such as benzocarbazoles and dibenzocarbazoles, respectively (Hughey et al., 2002; Shi et al., 2010; Oldenburg et al., 2014; Poetz et al., 2014). The DBE 9 group is interpreted as containing a carbazole core unit with long alkyl chains as deduced in many studies (Hughey et al., 2002; Poetz et al., 2014). The abundance of the DBE 9 group was lower than those of the DBE 12 and 15 classes, which are interpreted to reflect carbazoles with one or two additional benzene rings, respectively. The N_1-DBE classes increase with increasing maturation due to ongoing aromatization (Hughey et al., 2004; Oldenburg et al., 2014). Thus, the N_1 species with DBE 9, 12 and 15 can be used to assess the maturity of the FI oil using a triangular plot (Oldenburg et al., 2014). The maturity of MX FI oil could therefore be assessed to be around 1% R_e (vitrinite reflectance equivalent) (Fig. 6). In corroboration with this result, the maturity of the MX FI oil calculated from the Methyl Phenanthrene Index (MPI-1) ratio (Radke, 1983) detected by GC-MS (Table 2)

462 was 0.97% suggesting a good thermal maturity assessment from the FI oils for the
463 MX sample.
464
465 *Sulfur-containing compounds in inclusion oils as potential maturity markers*
466 S_1 compounds in the MX sample had a broad DBE range from 1 to 26, and
467 carbon numbers between 14 and 70 (Fig. 7). Compared to other reported crude oils
468 (Purcell et al., 2007; Liu et al., 2010; Walters et al., 2015), the MX FI oil contained
469 much broader carbon number and DBE ranges for the S_1 compounds. DBE 1 can be
470 interpreted to be alkyl thiolanes (tetrahydrothiophenes) or alkyl thianes
471 (tetrahydrothiopyrans), and DBE 2 with an additional fused naphthenic ring, while the
472 DBE 3 class might bear a thiophene unit (Liu et al., 2018). DBE 4 and 5 classes
473 presumably consist of thiophene with additional naphthenic rings. However, DBE 6
474 and DBE 9 classes were preferentially enriched probably containing compounds
475 consisting of a thiophene unit and additional benzene rings such as known from
476 benzothiophenes (BTs) and dibenzothiophenes (DBTs), respectively (Ho et al., 1974;
477 Griffiths et al., 2013; Walters et al., 2015). The presence of DBTs are confirmed by
478 GC-MS. In general, DBTs represent more thermally stable organosulfur compounds
479 than do the low DBE S_1 compounds (BTs, thiophenes and alkylsulfides) (Ho et al.,
480 1974; Manzano et al., 1997). It was observed that the abundance of low DBE S_1
481 compounds decreases with increasing maturity, while those of high DBE S_1
482 compounds increased in crude oil (Li et al., 2011; Oldenburg et al., 2014). Oldenburg
483 et al. (2014) reported that low DBE sulfur compounds (lower than 5) were absent

484 from maturity 0.68% to 1.1%. According to the N_1 compounds and MPI ratio shown
485 above, the thermal maturity of the MX sample was roughly estimated around 1% R_e.
486 It is remarkable that despite its peak oil window maturity level high abundances of S_1
487 species with low DBE values can still be observed. Two reasons might be responsible
488 for this: 1) the aromatization process for the N_1 compounds is faster indicating
489 different transformation gradients for N_1 versus S_1 compounds or 2) the S_1 compound
490 distribution might be influenced by generation of lower DBE S_1 compounds. A
491 conceivable process for the addition of low DBE S_1 compounds could be
492 thermochemical sulfate reduction (TSR), during which low DBE organosulfur
493 compounds are formed faster than they are destroyed, and similar cases have been
494 described in studies reported by Li et al. (2011) and Walters et al., (2015). The TSR
495 process has been confirmed in the MX fluorite by the presence of hydrogen sulfide in
496 fluid inclusions detected by Raman spectroscopy, and the presence of by-products
497 from TSR e.g., calcite inclusions, solid bitumen (González-Partida et al., 2003; Tritlla
498 et al., 2004). It is reasonable to deduce that TSR was responsible for the anomalous S_1
499 compounds distribution outlined above.

500 Our results show that, like the N_1 compounds, the S_1 components might also
501 have the potential to act as maturity indicators and that S_1 compounds can be
502 investigated in oil inclusions. However, their range of applicability and the factors
503 influencing this parameter have still to be tested and evaluated with a larger number
504 of sulfur containing samples.
505

Hydrocarbons in inclusion oils

Due to its ionization limitations, not all unsaturated and aromatic hydrocarbons can be ionized in APPI (+) mode (Marshall and Rodgers, 2008). Nevertheless, hydrocarbons were detected in all four investigated samples (Table 3). The carbon number range increases from the GE to the TN, PK and MX samples (Fig. 4b, 8). Thus, the PK and MX sample represent the broadest DBE and carbon number range. The DBE distribution of the GE FI oil showed a range from 3 to 13, while in the TN, MX and PK samples DBE was significantly higher, namely 26, 27 and 31, respectively (Fig. 4b, 8). This order is in accordance with the maturity assessment calculated by MPI-1 for the FI oils (GE (0.78%), TN (0.93%), MX (0.97%) and PK (1.31%); Table 2), in which higher maturity inclusion oils shows higher DBE numbers. This indicates an increasing degree of aromaticity with increasing maturation.

Additionally, the carbon number range increases from the GE to the TN, PK and MX samples. Thus, the PK and MX sample represent the broadest DBE and carbon number range. In figure 9 different patterns in the carbon number distribution of the DBE 5 group of the four investigated samples are presented (Oldenburg et al., 2014). The GE and TN sample patterns ranged from 15 to 41 or 45 carbon atoms and showed a maximum at C_{29}. In contrast, the carbon number distribution in the PK and MX samples was broader ranging from 15 to 60 or 65 carbon atoms with a broad maximum between C_{25}-C_{40}. The GE and TN type distribution is similar to that reported for oils with a lower maturity and a maximum at C_{29} as well as a rapid decline from C_{29} to C_{30} (Oldenburg et al., 2014). In contrast, the PK and MX

distribution pattern with the broader maximum around C_{33} resemble oils with higher maturity (Oldenburg et al., 2014). Thus, these data suggest that the PK and MX FI oils show a higher maturity than the GE and TN samples. In principle this coincides with the calculated maturity assessment based on MPI-1. However, TN and MX show only low calculated maturity differences (TN 0.93 % R_c and MX 0.97% R_c), but significant different DBE 5 group distributions (Fig. 9), indicating that also other factors than only thermal maturity (e.g., facies differences) might play a role for the different DBE 5 distributions.

3.4.3 Potential to infer biodegradation levels from inclusion oils

The particular strength of the FI method is to provide crucial information on the original oil composition and oil properties, especially when the reservoir oil has been altered by biodegradation. Importantly, the FI oils can also be used to search for early indications of oil biodegradation. Oxygen compounds, especially O_1 and O_2 compounds, measured by the ESI (-) mode have been widely studied and relationships between those compound class compositions and biodegradation have been demonstrated (Kim et al., 2005; Liao et al., 2012; Noah et al., 2015; Martins et al., 2017). It is known from previous ESI FT-ICR-MS based investigations of crude oils, that the abundance of O_2 species increase while those of the O_1 species decrease with increasing level of biodegradation (Kim et al., 2005; Hughey et al., 2007). Thus, the relative proportion of O_1 to O_2 compounds can provide a first hint for biodegradation. O_2 compounds are abundant, especially those from DBE 1 class representing acyclic

carboxylic acids (Kim et al., 2005). In contrast, O_2 compounds with DBE 2, 3 and 4 represent mono-, bi- and tricyclic naphthenic acids (Kim et al., 2005; Noah et al., 2015). Kim et al. (2005) introduced the A/C (acyclic/cyclic) ratio ($A/C = \sum O_{2,\ DBE1}/\sum O_{2,\ DBE2+3+4}$) to estimate potential biodegradation levels of crude oil. The A/C ratio decreases with increasing biodegradation due to relative increase of cyclic acids and decrease of acyclic fatty acids. The A/C ratio has successfully been applied to access biodegradation levels in petroleum reservoirs and at remediation sites (Kim et al., 2005; Liao et al., 2012; Martins et al., 2017; Noah et al., 2015).

Both the O_1 and O_2 compound classes were detected in the FI oils of the PK sample (Table 3). O_1 species are suggested to contain a hydroxyl functional group, with the DBE value ranges from 1 to 14 and carbon numbers range from 13 to 33 (Fig. 10a). O_2 species in the PK sample, representing the most abundant oxygen containing compound class showed DBEs from 1 to 13, and carbon numbers range from 11 to 47 (Fig. 10b). O_2 species are strongly dominated by the DBE 1 group compounds, which represent carboxylic acids. While palmitic acid (C_{16}) and stearic acid (C_{18}) were detected in the blanks O_2 species in the PK sample show overall only a low level of contamination (category II), and thus the O_2 data can be used to assess the A/C ratio. Compared with the findings about O_2 species in literature (Liao et al. (2012), Kim et al. (2005), Noah et al. (2015) and Martins et al. (2017)) a A/C ratio of 1.6 indicates that the inclusion oil in the PK sample can be assessed as non-biodegraded during the time of trapping in the FI. This result was confirmed by GC-MS data showing an unaffected *n*-alkane distribution pattern and the absence of an unresolved complex

mixture (UCM). Although the investigated sample shows no indication for an early biodegradation, this example indicates that the respective compounds for a biodegradation assessment can be detected from FI oils using the FT-ICR-MS. Thus, the new method shows high potential for indicating biodegradation in oil inclusions.

Conclusion and outlook

A clean-up and crushing procedure for different host minerals has been developed, enabling biomolecules and NSO-compounds in oil-bearing fluid inclusions to be analyzed using FT-ICR-MS (APPI (+) and ESI (-) ionization modes) and GC-MS as well. An additional putative benefit of the presented procedure is that it can also be applied to carbonate mineral hosts since it does not employ acids.

Although external contamination cannot completely be removed by the clean-up procedure in all cases, especially where extraction yields are low, the developed method allows the contamination levels of different compound classes to be assessed and classified. This classification allows samples to be screened as to whether they are suitable or unsuitable for detailed interpretation. Data evaluation showed that the main compound classes are less influenced by external contamination especially in the APPI (+) mode and that their abundance in fluid inclusions allows the established parameters for oil characterization to be determined. With this method a new window is opened to investigate NSO compounds in fluid inclusions with the FT-ICR-MS technique and to get more comprehensive information on petroleum and/or economic mineral emplacement.

Acknowledgements

The China Scholarship Council (CSC) is gratefully acknowledged for funding Yufu Han's research. We are indebted to Nicole Guilhaumou (Museum d'Histoire Naturelle Paris), David Banks (University of Leeds) and Stephen Becker (ExxonMobil Upstream Research Company) for providing sample material. We extend our gratitude to Cornelia Karger and Anke Kaminsky for their technical support. We are grateful to John Volkman, Herbert Volk, Paul Greenwood and an anonymous reviewer for their careful and constructive reviews of this paper.

References

Benchilla, L., Guilhaumou, N., Mougin, P., Jaswal, T., Roure, F., 2003. Reconstruction of palaeo-burial history and pore fluid pressure in foothill areas: a sensitivity test in the Hammam Zriba (Tunisia) and Koh-i-Maran (Pakistan) ore deposits. Geofluids 3, 103-123.

Betz, D., Führer, F., Greiner, G., Plein, E., 1987. Evolution of the Lower Saxony basin. Tectonophysics 137, 127-170.

Bodnar, R.J., 1990. Petroleum migration in the Miocene Monterey Formation, California, USA: constraints from fluid inclusion studies. Mineralogical magazine 54, 295-304.

Bouhlel, S., Fortuné, J.P., Guilhaumou, N., Touray, J.C., 1988. Les minéralisations stratiformes à F-Ba de Hammam Zriba, Jebel Guébli (Tunisie nord orientale):

615 l'apport des études d'inclusions fluides à la modélisation génétique. Mineralium
616 Deposita 23, 166-173.
617 Burruss, R.C., 1981. Hydrocarbon fluid inclusions in studies of sedimentary
618 diagenesis. Fluid inclusions: Applications to petrology, Vol. Short Course Notes
619 6, 138-156.
620 Burruss, R.C., 2003. Petroleum fluid inclusions, an introduction. Fluid Inclusions:
621 Analysis and Interpretation. Edited by I. Samson, A. Anderson, and D. Marshall.
622 Mineralogical Association of Canada, Short Course Ser 32, 159-174.
623 Burruss, R.C., Cercone, K.R., Harris, P.M., 1985. Timing of hydrocarbon migration:
624 evidenced from fluid inclusions in calcite cements, tectonics and burial history.
625 Society of Economic Paleontologists and Mineralogists Special Publication 36,
626 277-289.
627 Cathles, L., Smith, A., 1983. Thermal constraints on the formation of Mississippi
628 Valley-type lead-zinc deposits and their implications for episodic basin
629 dewatering and deposit genesis. Economic Geology 78, 983-1002.
630 Crocker, M., Marchin, L., 1988. Wettability and adsorption characteristics of
631 crude-oil asphaltene and polar fractions. Journal of petroleum technology 40,
632 470-474.
633 Etminan, H., Hoffmann, C.F., 1989. Biomarkers in fluid inclusions: A new tool in
634 constraining source regimes and its implications for the genesis of Mississippi
635 Valley-type deposits. Geology 17, 19-22.
636 George, S.C., Ahmed, M., Liu, K., Volk, H., 2004. The analysis of oil trapped during

637 secondary migration. Organic Geochemistry 35, 1489-1511.
638 George, S.C., Krieger, F.W., Eadington, P.J., Quezada, R.A., Greenwood, P.F.,
639 Eisenberg, L.I., Hamilton, P.J., Wilson, M.A., 1997. Geochemical comparison of
640 oil-bearing fluid inclusions and produced oil from the Toro sandstone, Papua
641 New Guinea. Organic Geochemistry 26, 155-173.
642 George, S.C., Lisk, M., Summons, R.E., Quezada, R.A., 1998. Constraining the oil
643 charge history of the South Pepper oilfield from the analysis of oil-bearing fluid
644 inclusions. Organic Geochemistry 29, 631-648.
645 George, S.C., Volk, H., Ahmed, M., 2007. Geochemical analysis techniques and
646 geological applications of oil-bearing fluid inclusions, with some Australian case
647 studies. Journal of Petroleum Science and Engineering 57, 119-138.
648 Goldstein, H., 1994. Systematics of fluid inclusions in diagenetic minerals. SEPM
649 short course 31, 1-199.
650 González-Partida, E., Carrillo-Chávez, A., Grimmer, J., Pironon, J., 2002.
651 Petroleum-rich fluid inclusions in fluorite, Purisima mine, Coahuila, Mexico.
652 International Geology Review 44, 755-764.
653 González-Partida, E., Carrillo-Chávez, A., Grimmer, J., Pironon, J., Mutterer, J.,
654 Levresse, G., 2003. Fluorite deposits at Encantada-Buenavista, Mexico: products
655 of Mississippi Valley type processes. Ore Geology Reviews 23, 107-124.
656 Griffiths, M.T., Da Campo, R., O'Connor, P.B., Barrow, M.P., 2013. Throwing light
657 on petroleum: simulated exposure of crude oil to sunlight and characterization
658 using atmospheric pressure photoionization Fourier transform ion cyclotron

659 resonance mass spectrometry. Analytical chemistry 86, 527-534.
660 Guilhaumou, N., Ellouz, N., Jaswal, T., Mougin, P., 2000. Genesis and evolution of
661 hydrocarbons entrapped in the fluorite deposit of Koh-i-Maran, (North Kirthar
662 Range, Pakistan). Marine and Petroleum Geology 17, 1151-1164.
663 Han, Y., Poetz, S., Mahlstedt, N., Karger, C., Horsfield, B., 2018. Fractionation of
664 pyrrolic nitrogen compounds during primary migration of petroleum within the
665 Barnett Shale sequence of Marathon 1 Mesquite Well, Texas. Energy & Fuels 32,
666 4638-4650.
667 Ho, T., Rogers, M., Drushel, H., Koons, C., 1974. Evolution of sulfur compounds in
668 crude oils. AAPG Bulletin 58, 2338-2348.
669 Horsfield, B., McLimans, R., 1984. Geothermometry and geochemistry of aqueous
670 and oil-bearing fluid inclusions from Fateh Field, Dubai. Organic Geochemistry
671 6, 733-740.
672 Huang, H., Bowler, B.F., Zhang, Z., Oldenburg, T.B., Larter, S.R., 2003. Influence of
673 biodegradation on carbazole and benzocarbazole distributions in oil columns
674 from the Liaohe basin, NE China. Organic Geochemistry 34, 951-969.
675 Hughey, C.A., Galasso, S.A., Zumberge, J.E., 2007. Detailed compositional
676 comparison of acidic NSO compounds in biodegraded reservoir and surface
677 crude oils by negative ion electrospray Fourier transform ion cyclotron resonance
678 mass spectrometry. Fuel 86, 758-768.
679 Hughey, C.A., Rodgers, R.P., Marshall, A.G., Qian, K., Robbins, W.K., 2002.
680 Identification of acidic NSO compounds in crude oils of different geochemical

origins by negative ion electrospray Fourier transform ion cyclotron resonance mass spectrometry. Organic Geochemistry 33, 743-759.

Hughey, C.A., Rodgers, R.P., Marshall, A.G., Walters, C.C., Qian, K.N., Mankiewicz, P., 2004. Acidic and neutral polar NSO compounds in Smackover oils of different thermal maturity revealed by electrospray high field Fourier transform ion cyclotron resonance mass spectrometry. Organic Geochemistry 35, 863-880.

Jones, D., Macleod, G., 2000. Molecular analysis of petroleum in fluid inclusions: a practical methodology. Organic Geochemistry 31, 1163-1173.

Karlsen, D.A., Nedkvitne, T., Larter, S.R., Bjørlykke, K., 1993. Hydrocarbon composition of authigenic inclusions: Application to elucidation of petroleum reservoir filling history. Geochimica et Cosmochimica Acta 57, 3641-3659.

Kim, S., Stanford, L.A., Rodgers, R.P., Marshall, A.G., Walters, C.C., Qian, K., Wenger, L.M., Mankiewicz, P., 2005. Microbial alteration of the acidic and neutral polar NSO compounds revealed by Fourier transform ion cyclotron resonance mass spectrometry. Organic Geochemistry 36, 1117-1134.

Li, S., Pang, X., Shi, Q., Zhang, B., Zhang, H., Pan, N., Zhao, M., 2011. Origin of the unusually high dibenzothiophene concentrations in Lower Ordovician oils from the Tazhong Uplift, Tarim Basin, China. Petroleum Science 8, 382-391.

Liao, Y., Shi, Q., Hsu, C.S., Pan, Y., Zhang, Y., 2012. Distribution of acids and nitrogen-containing compounds in biodegraded oils of the Liaohe Basin by negative ion ESI FT-ICR MS. Organic Geochemistry 47, 51-65.

Lisk, M., George, S., Summons, R., Quezada, R., O'Brien, G., 1996. Mapping

703 hydrocarbon charge histories: detailed characterisation of the South Pepper oil
704 field, Carnarvon Basin. The APPEA journal 36, 445-464.
705 Liu, P., Li, M., Jiang, Q., Cao, T., Sun, Y., 2015. Effect of secondary oil migration
706 distance on composition of acidic NSO compounds in crude oils determined by
707 negative-ion electrospray Fourier transform ion cyclotron resonance mass
708 spectrometry. Organic Geochemistry 78, 23-31.
709 Liu, P., Xu, C., Shi, Q., Pan, N., Zhang, Y., Zhao, S., Chung, K.H., 2010.
710 Characterization of sulfide compounds in petroleum: selective oxidation
711 followed by positive-ion electrospray Fourier transform ion cyclotron resonance
712 mass spectrometry. Analytical Chemistry 82, 6601-6606.
713 Liu, W., Liao, Y., Pan, Y., Jiang, B., Zeng, Q., Shi, Q., Hsu, C.S., 2018. Use of ESI
714 FT-ICR MS to investigate molecular transformation in simulated aerobic
715 biodegradation of a sulfur-rich crude oil. Organic Geochemistry 123, 17-26.
716 Lüders, V., Plessen, B., 2015. Stable carbon isotope ratios of CH_4-rich gas inclusions
717 in shale-hosted fracture-fill mineralization: A tool for tracing hydrocarbon
718 generation and migration in shale plays for oil and gas. Marine and Petroleum
719 Geology 63, 68-81.
720 Lüders, V., Plessen, B., di Primio, R., 2012. Stable carbon isotopic ratios of
721 CH_4-CO_2-bearing fluid inclusions in fracture-fill mineralization from the Lower
722 Saxony Basin (Germany) - A tool for tracing gas sources and maturity. Marine
723 and Petroleum Geology 30, 174-183.
724 Mahlstedt, N., Horsfield, B., Wilkes, H., Poetz, S., 2016. Tracing the impact of fluid

725 retention on bulk petroleum properties using nitrogen-containing compounds.
726 Energy & Fuels 30, 6290-6305.
727 Manzano, B., Fowler, M., Machel, H., 1997. The influence of thermochemical
728 sulphate reduction on hydrocarbon composition in Nisku reservoirs, Brazeau
729 river area, Alberta, Canada. Organic Geochemistry 27, 507-521.
730 Marshall, A.G., Rodgers, R.P., 2004. Petroleomics: the next grand challenge for
731 chemical analysis. Accounts of Chemical Research 37, 53-59.
732 Marshall, A.G., Rodgers, R.P., 2008. Petroleomics: Chemistry of the underworld.
733 Proceedings of the National Academy of Sciences 105, 18090-18095.
734 Martins, L.L., Pudenzi, M.A., da Cruz, G.F., Nascimento, H.D., Eberlin, M.N., 2017.
735 Assessing biodegradation of Brazilian crude oils via characteristic profiles of O_1
736 and O_2 compound classes: Petroleomics by negative-ion mode electrospray
737 ionization Fourier transform ion cyclotron resonance mass spectrometry. Energy
738 & Fuels 31, 6649-6657.
739 McLimans, R.K., 1987. The application of fluid inclusions to migration of oil and
740 diagenesis in petroleum reservoirs. Applied Geochemistry 2, 585-603.
741 Munz, I.A., 2001. Petroleum inclusions in sedimentary basins: systematics, analytical
742 methods and applications. Lithos 55, 195-212.
743 Murray, R.C., 1957. Hydrocarbon fluid inclusions in quartz. AAPG Bulletin 41,
744 950-952.
745 Nedkvitne, T., Karlsen, D.A., Bjørlykke, K., Larter, S.R., 1993. Relationship between
746 reservoir diagenetic evolution and petroleum emplacement in the Ula Field,

North Sea. Marine and Petroleum Geology 10, 255-270.

Nichols, D., 2019. How to clean rocks and crystals, https://www.canoncitygeologyclub.com/uploads/4/5/5/2/45523343/how_to_clean_minerals_and_crystals.pdf.

Noah, M., Poetz, S., Vieth-Hillebrand, A., Wilkes, H., 2015. Detection of residual oil-sand-derived organic material in developing soils of reclamation sites by ultra-high-resolution mass spectrometry. Environmental science & technology 49, 6466-6473.

Noah, M., Volk, H., Schubert, F., Horsfield, B., 2018. First analysis of polar compounds trapped in fluid inclusions using ultra high resolution mass spectrometry – A proof of concept demonstrated on a case study from the Pannonian Basin (Hungary), Latin American Association of Organic Geochemistry (ALAGO), Salvador, Bahia, Brazil.

Noah, M., Volk, H., Schubert, F., Horsfield, B., 2019. Identification of NSO Compounds Trapped in Fluid Inclusions Using FT-ICR-MS - A Case Study from the Pannonian Basin (Hungary), 29th International Meeting on Organic Geochemistry, Gothenburg, Sweden.

Oldenburg, T.B., Jones, M., Huang, H., Bennett, B., Shafiee, N.S., Head, I., Larter, S.R., 2017. The controls on the composition of biodegraded oils in the deep subsurface - Part 4. Destruction and production of high molecular weight non-hydrocarbon species and destruction of aromatic hydrocarbons during progressive in-reservoir biodegradation. Organic Geochemistry 114, 57-80.

769 Oldenburg, T.B.P., Brown, M., Bennett, B., Larter, S.R., 2014. The impact of thermal
770 maturity level on the composition of crude oils, assessed using ultra-high
771 resolution mass spectrometry. Organic Geochemistry 75, 151-168.
772 Oliveros, J.C., 2007. VENNY. An interactive tool for comparing lists with Venn
773 Diagrams. http://bioinfogp. cnb. csic. es/tools/venny/index. html.
774 Pang, L.S.K., George, S.C., Quezada, R.A., 1998. A study of the gross compositions
775 of oil-bearing fluid inclusions using high performance liquid chromatography.
776 Organic Geochemistry 29, 1149-1161.
777 Peters, C.A., Hallmann, C., George, S.C., 2018. Phenolic compounds in oil-bearing
778 fluid inclusions: Implications for water-washing and oil migration. Organic
779 Geochemistry 118, 36-46.
780 Poetz, S., Horsfield, B., Wilkes, H., 2014. Maturity-driven generation and
781 transformation of acidic compounds in the organic-rich Posidonia shale as
782 revealed by electrospray ionization Fourier transform ion cyclotron resonance
783 mass spectrometry. Energy & Fuels 28, 4877-4888.
784 Purcell, J.M., Hendrickson, C.L., Rodgers, R.P., Marshall, A.G., 2006. Atmospheric
785 pressure photoionization Fourier transform ion cyclotron resonance mass
786 spectrometry for complex mixture analysis. Analytical Chemistry 78, 5906-5912.
787 Purcell, J.M., Juyal, P., Kim, D.-G., Rodgers, R.P., Hendrickson, C.L., Marshall, A.G.,
788 2007. Sulfur speciation in petroleum: Atmospheric pressure photoionization or
789 chemical derivatization and electrospray ionization Fourier transform ion
790 cyclotron resonance mass spectrometry. Energy & Fuels 21, 2869-2874.

791 Radke, M., 1983. The methylphenanthrene index (MPI): a maturity parameter based
792 on aromatic hydrocarbons. Advances Organic Geochemistry 1981, 504-512.
793 Rodgers, R.P., Marshall, A.G., 2007. Petroleomics: Advanced characterization of
794 petroleum-derived materials by Fourier transform ion cyclotron resonance mass
795 spectrometry (FT-ICR MS), Asphaltenes, Heavy Oils, and Petroleomics.
796 Springer, New York, pp. 63-93.
797 Roedder, E., 1984. Fluid inclusions, Mineralogical Society of America, Washington,
798 DC.
799 Ruble, T.E., George, S.C., Lisk, M., Quezada, R.A., 1998. Organic compounds
800 trapped in aqueous fluid inclusions. Organic Geochemistry 29, 195-205.
801 Seidel, M., Kleindienst, S., Dittmar, T., Joye, S.B., Medeiros, P.M., 2016.
802 Biodegradation of crude oil and dispersants in deep seawater from the Gulf of
803 Mexico: Insights from ultra-high resolution mass spectrometry. Deep Sea
804 Research Part II: Topical Studies in Oceanography 129, 108-118.
805 Shi, Q., Zhao, S., Xu, Z., Chung, K., Zhang, Y., Xu, C., 2010. Distribution of acids
806 and neutral nitrogen compounds in a Chinese crude oil and its fractions:
807 characterized by negative-ion electrospray ionization fourier transform ion
808 cyclotron resonance mass spectrometry. Energy & Fuels 24, 4005-4011.
809 Siljeström, S., Lausmaa, J., Sjovall, P., Broman, C., Thiel, V., Hode, T., 2010.
810 Analysis of hopanes and steranes in single oil-bearing fluid inclusions using
811 time-of-flight secondary ion mass spectrometry (ToF-SIMS). Geobiology 8,
812 37-44.

Siljeström, S., Volk, H., George, S.C., Lausmaa, J., Sjövall, P., Dutkiewicz, A., Hode, T., 2013. Analysis of single oil-bearing fluid inclusions in mid-Proterozoic sandstones (Roper Group, Australia). Geochimica et Cosmochimica Acta 122, 448-463.

Tissot, B.P., Welte, D.H., 1984. Petroleum formation and occurrence. Springer Science & Business Media, New York, NY.

Tritlla, J., González-Partida, E., Levresse, G., Banks, D., Pironon, J., 2004. "Fluorite deposits at Encantada-Buenavista, Mexico: products of Mississippi Valley type processes"[Ore Geol. Rev. 23 (2003), 107–124] - a reply. Ore Geology Reviews 25, 329-332.

Ulrich, W., 1989. The quartz crystals of Herkimer County and its environs. Rocks & Minerals 64, 108-122.

Volk, H., Fuentes, D., Fuerbach, A., Miese, C., Koehler, W., Bärsch, N., Barcikowski, S., 2010. First on-line analysis of petroleum from single inclusion using ultrafast laser ablation. Organic geochemistry 41, 74-77.

Volk, H., George, S.C., 2019. Using petroleum inclusions to trace petroleum systems - A review. Organic Geochemistry 129, 99-123.

Volk, H., Horsfield, B., Mann, U., Suchý, V., 2002. Variability of petroleum inclusions in vein, fossil and vug cements - a geochemical study in the Barrandian Basin (Lower Palaeozoic, Czech Republic). Organic Geochemistry 33, 1319-1341.

Walters, C.C., Wang, F.C., Qian, K., Wu, C., Mennito, A.S., Wei, Z., 2015.

Petroleum alteration by thermochemical sulfate reduction - A comprehensive molecular study of aromatic hydrocarbons and polar compounds. Geochimica et Cosmochimica Acta 153, 37-71.

Zhang, Z., Greenwood, P., Zhang, Q., Rao, D., Shi, W., 2012. Laser ablation GC–MS analysis of oil-bearing fluid inclusions in petroleum reservoir rocks. Organic Geochemistry 43, 20-25.

Ziegs, V., Noah, M., Poetz, S., Horsfield, B., Hartwig, A., Rinna, J., Skeie, J.E., 2018. Unravelling maturity- and migration-related carbazole and phenol distributions in Central Graben crude oils. Marine and Petroleum Geology 94, 114-130.

Table 1. Geological information about host mineral in various area

Sample name	Host mineral	Location	Formation Time	Host rock	Potential source rock
GE	quartz	Germany	Late Jurassic-Early Cretaceous	Triassic sandstone	Lower Jurassic Posidonia shale
TN	fluorite	Tunisia	Late Tortonian-Pliocene	Campanian and Tithonian series limestones	Triassic-Permian sediments
PK	quartz	Pakistan	Early Oligocene	Upper Jurassic limestones	Lower Jurassic sediments
MX	fluorite	Mexico	Tertiary	Upper Cretaceous shale and carbonates	Upper Jurassic Calcareous shale and carbonates

Table 2. Extraction yields and maturity related ratios of fluid inclusion oils.

Host mineral	Sample weight (g)	Extracted oil (mg)	Extracted oil (μg/g)	MPI-1	R_c (%)
GE-quartz	8.56	0.48	56	-	0.78#
TN-fluorite	2.38	0.38	159	0.88	0.93
PK-quartz	8.53	3.12	366	1.51	1.31
MX-fluorite	12.08	1.28	106	0.95	0.97

Note: GE and PK: quartz samples from Germany and Pakistan, respectively. TN and MX: fluorite samples from Tunisia and Mexico, respectively (see Table 1). Methylphenanthrene index (MPI-1) = 1.5 × [3MP + 2MP]/[P + 9MP + 1MP]; Calculated reflectance (R_c %) = 0.60 × MPI-1 + 0.40 (for 0.65% < R_o < 1.35%) (Radke, 1983). -: not detected; #: Phenanthrene was not detected in sample GE and thus, R_c was calculated based on carbon isotope ratio of methane in oil inclusions (Lüders et al. 2012).

Table 3. Classification of the main compound classes in the investigated inclusion oils (see Table 1) with regard to

their level of external contamination (after comparison with blanks).

Compounds classes	*APPI (+) mode*				*ESI (-) mode*			
	GE	TN	PK	MX	GE	TN	PK	MX
HC	II	II	II	II			#	
O_1	II	II	II	II	I	I	III	I
O_2	II	II	II	I	II	I	II	II
O_3	I	I	II	I	I	I	II	I
O_4	I	I	I	I	I	I	II	I
O_5	I	I	\	I	I	I	II	I
O_6	I	I	\	I	I	I	II	I
N_1	I	I	III	III	\	\	III	III
S_1	\	III	\	III			#	
S_2	\	I	\	III			#	
N_1S_1	\	\	\	III	\	\	\	III
N_1O_1	I	I	I	II	\	\	\	\
N_2O_2	I	I	I	I	I	I	I	I
S_1O_1	\	I	II	III	I	II	III	II

Note: I : detected compounds are not suitable for further interpretation (category I: highly contaminated), II : the overwhelming part of the compounds is unique to the FI oils (category II: low contamination level and conditionally suitable for further interpretation), III: compounds are unique to the FI oils (category III: not contaminated and fully suitable for further interpretation), \ : no compounds detected, # : compounds not ionizable in ESI (-) mode.

Figure

Fig. 1. Photographs of fluid inclusion samples: a) quartz vein material from a Upper

Triassic sandstone (Germany, GE); b) fluorite from Campanian series limestones (Tunisia, TN); c) quartz from Upper Jurassic limestones (Pakistan, PK); d) fluorite from Upper Cretaceous shale and carbonates (Mexico, MX).

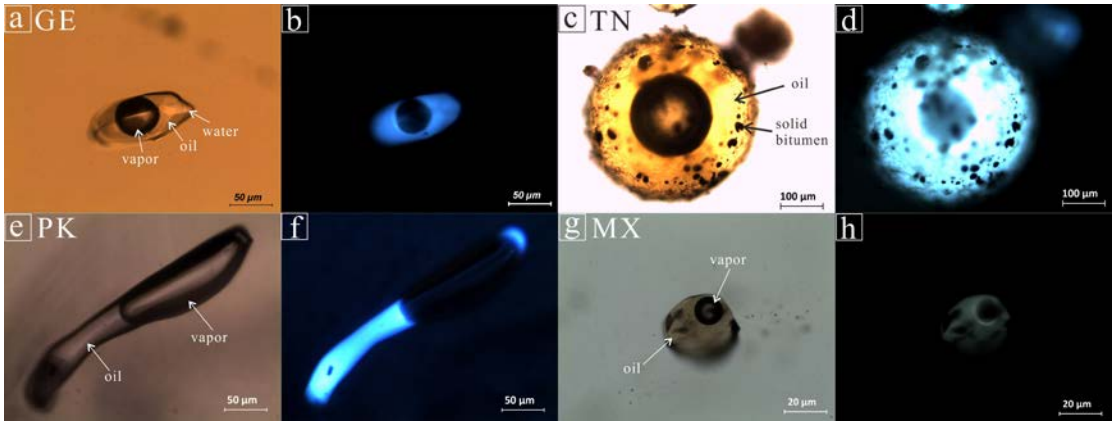

Fig. 2. Photomicrographs of oil-bearing fluid inclusions under transmitted (a, c, e and g) and UV light (b, d, f and h). GE and PK: quartz sample from Germany and Pakistan, respectively. TN and MX: fluorite samples from Tunisia and Mexico, respectively (see Table 1).

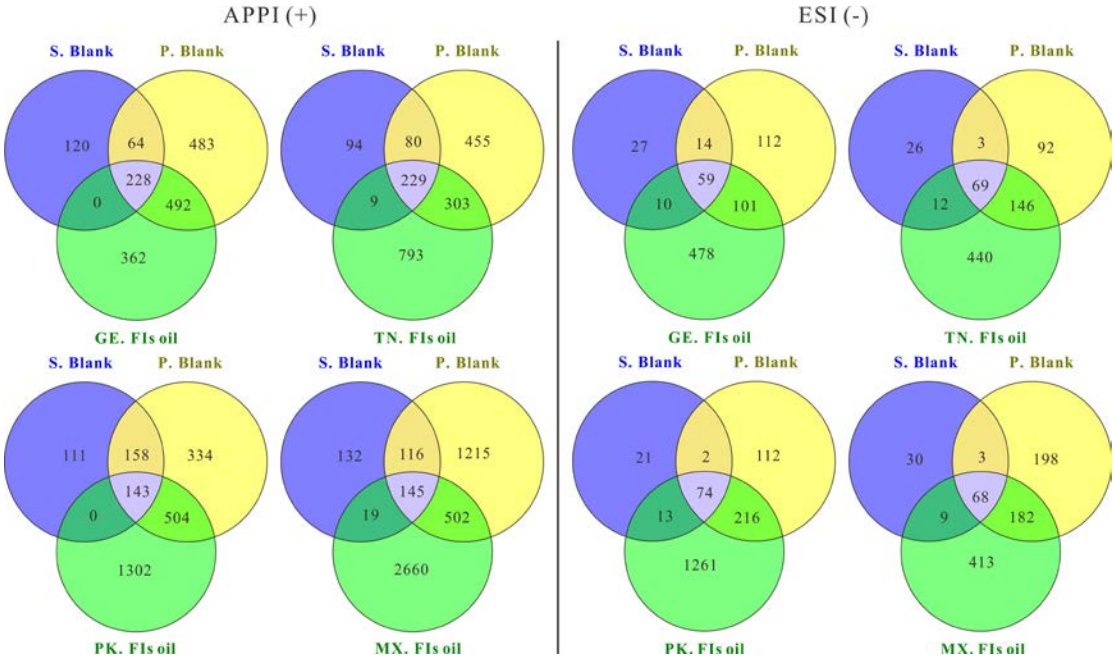

Fig. 3. Venn diagrams showing the comparison of signals in system blank (S-blank),

procedural blank (P-blank) and inclusion oils (FI). Non-overlapping areas indicate signals being unique to a sample type, overlapping areas indicate common signals between two or all sample types. Left side FT-ICR-MS measurement in the APPI (+) mode and right side in the ESI (-) mode. GE and PK: quartz samples from Germany and Pakistan, respectively. TN and MX: fluorite samples from Tunisia and Mexico, respectively (see Table 1).

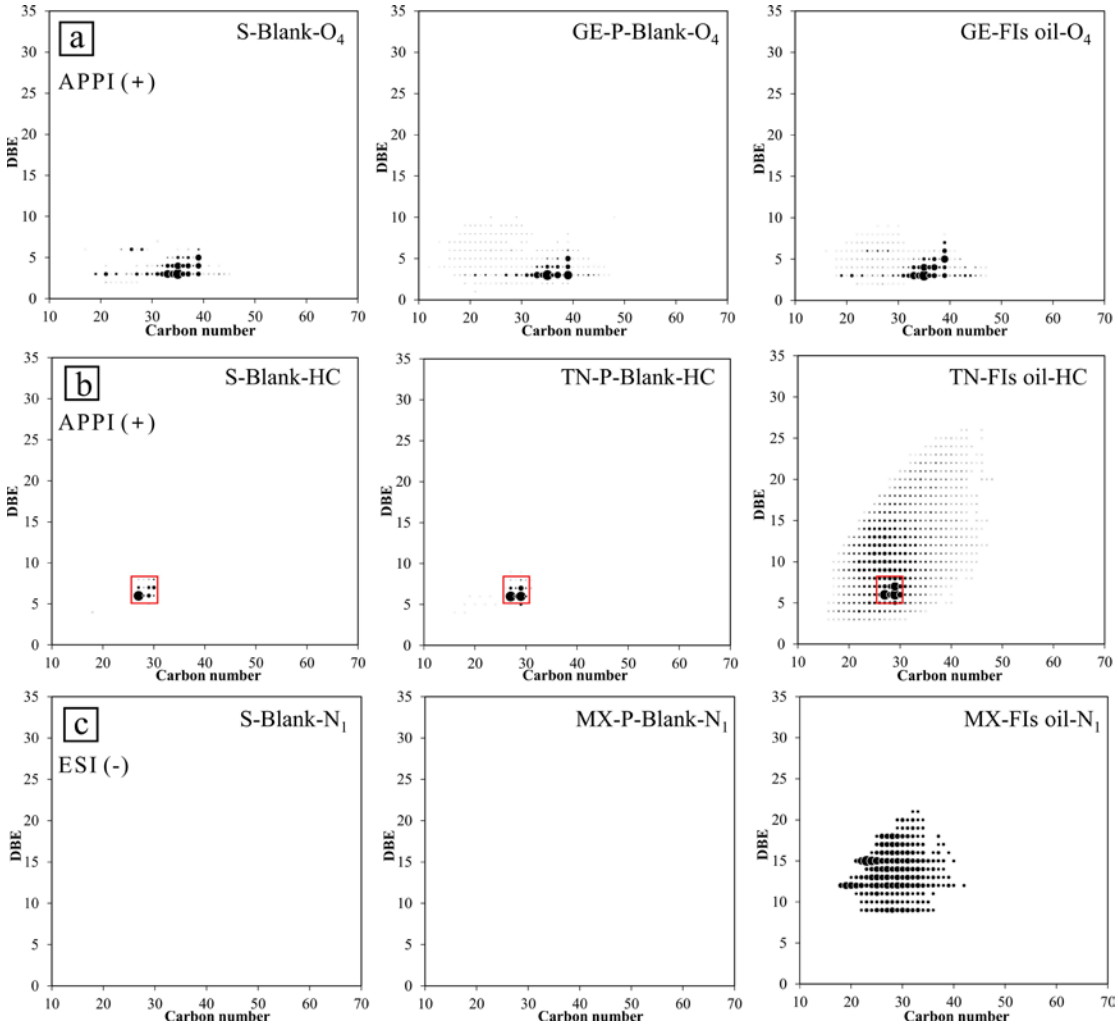

Fig. 4. DBE versus carbon number plots of the a) O_4, b) hydrocarbons (HC) and c) N_1 compound classes in the S-blank, P-blank and extract oil of a) the GE quartz sample b) and TN fluorite sample measured by FT-ICR-MS in the APPI (+) mode as well as c) the MX fluorite sample measured in the ESI (-) mode.

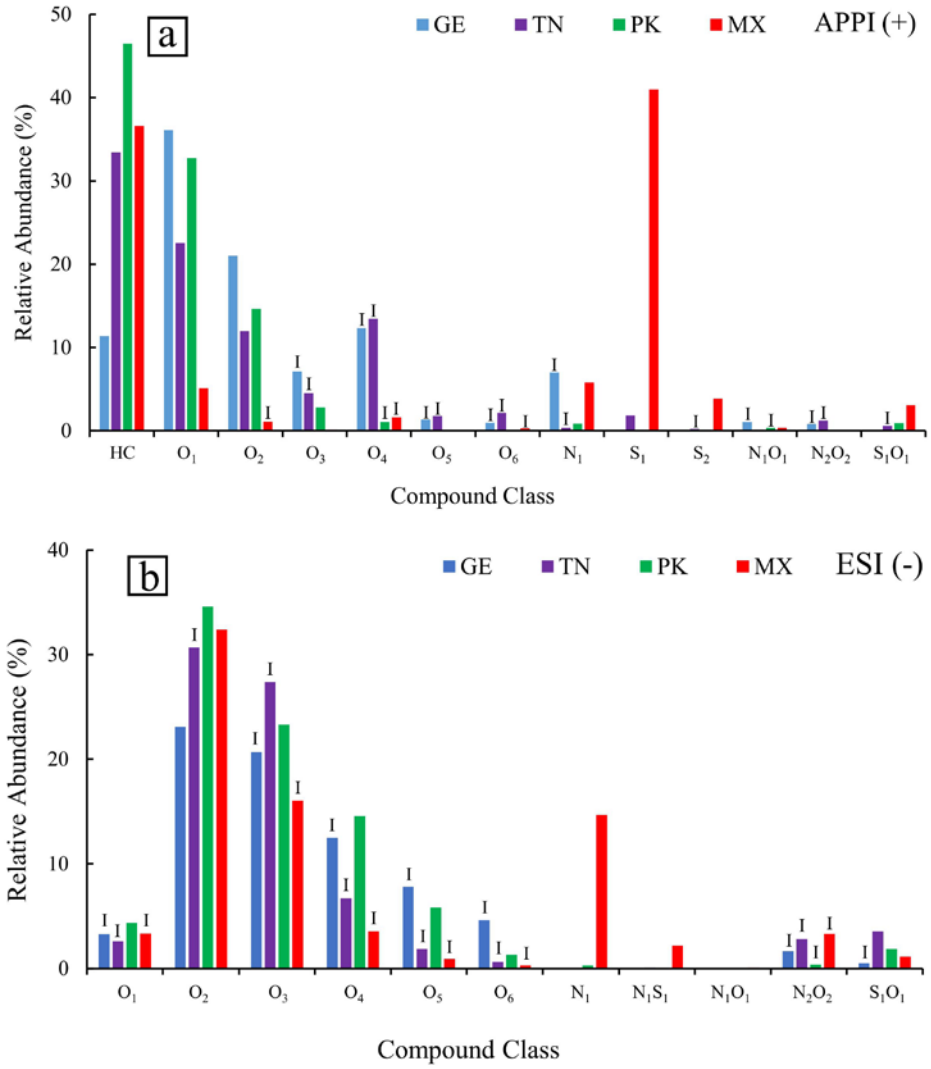

888

889 Fig. 5. Relative abundance of the compound classes of the four investigated FI oils

890 (see Table 1) measured by FT-ICR-MS in a) the APPI (+) and b) ESI (-) mode.

891 HC = hydrocarbons; element + number x = compounds bearing x hetero-atoms.

892 Strongly contaminated compound classes are marked with a “I”

893 (contamination category I). Sample types see Table 1.

894

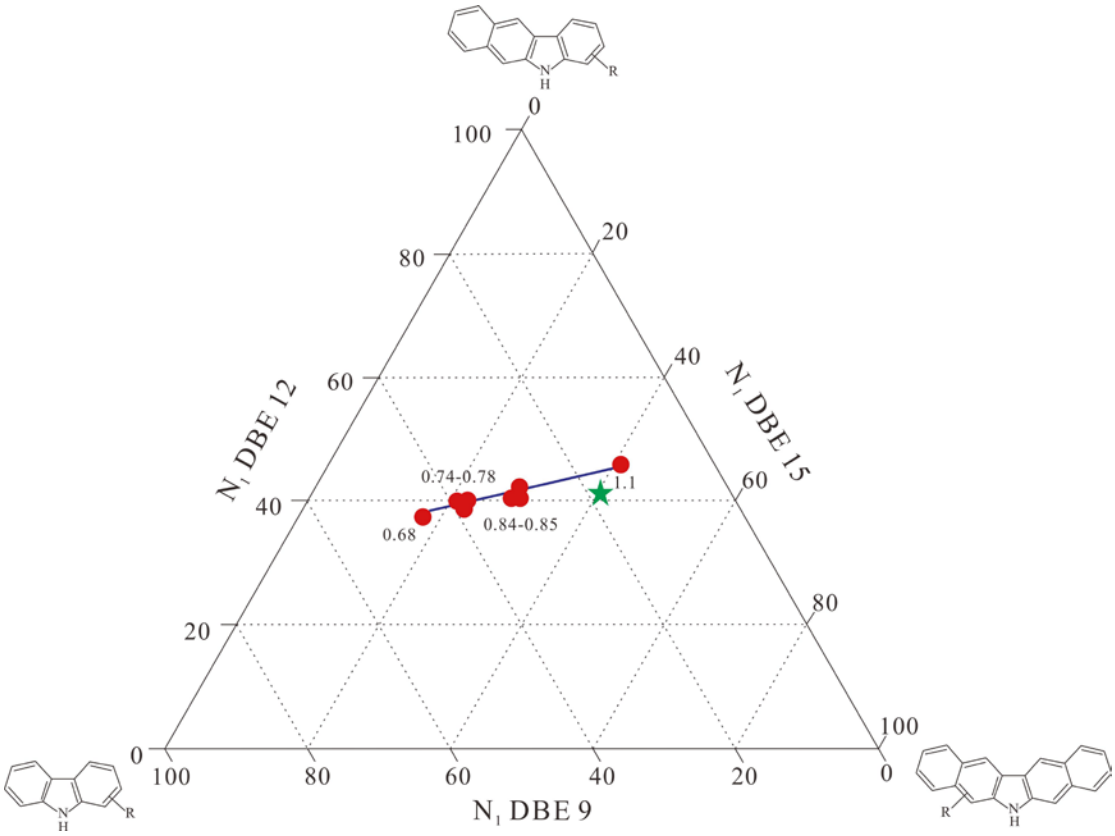

Fig. 6. Triangular plot of N_1 DBE 9, DBE 12 and DBE 15 (modified after Oldenburg et al. (2014)) representing carbazoles with increasing number of aromatic rings, which is maturity dependent. The red circles are samples from Oldenburg et al. (2014) indicating different vitrinite reflectance ranges. The green star represents the position of the MX fluid inclusion oil sample. DBE = double bond equivalent. N_1 = compounds group containing one nitrogen.

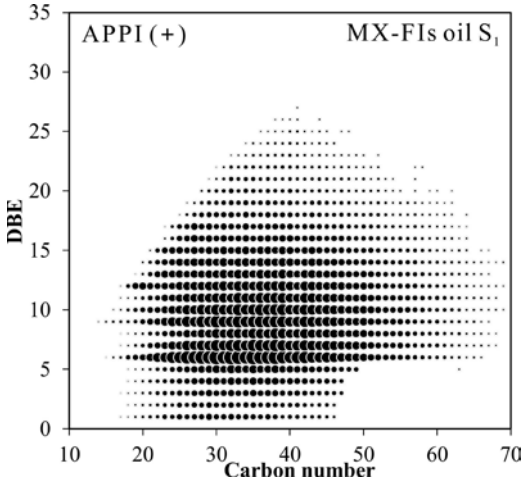

Fig. 7. Double bond equivalence (DBE) versus carbon number plot of S_1 compounds in the MX sample measured in APPI (+) mode.

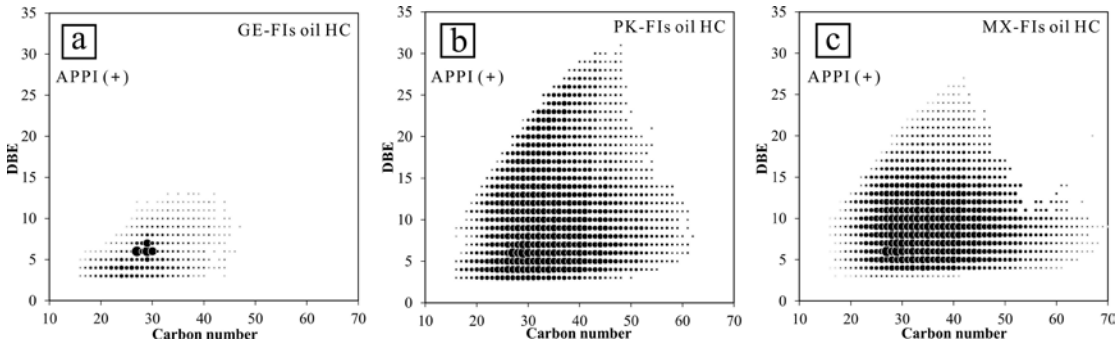

Fig. 8. Double bond equivalence (DBE) versus carbon number plots of HC in the inclusion oil samples a) GE, b) PK and c) MX measured in the APPI (+) mode. Sample types see Table 1.

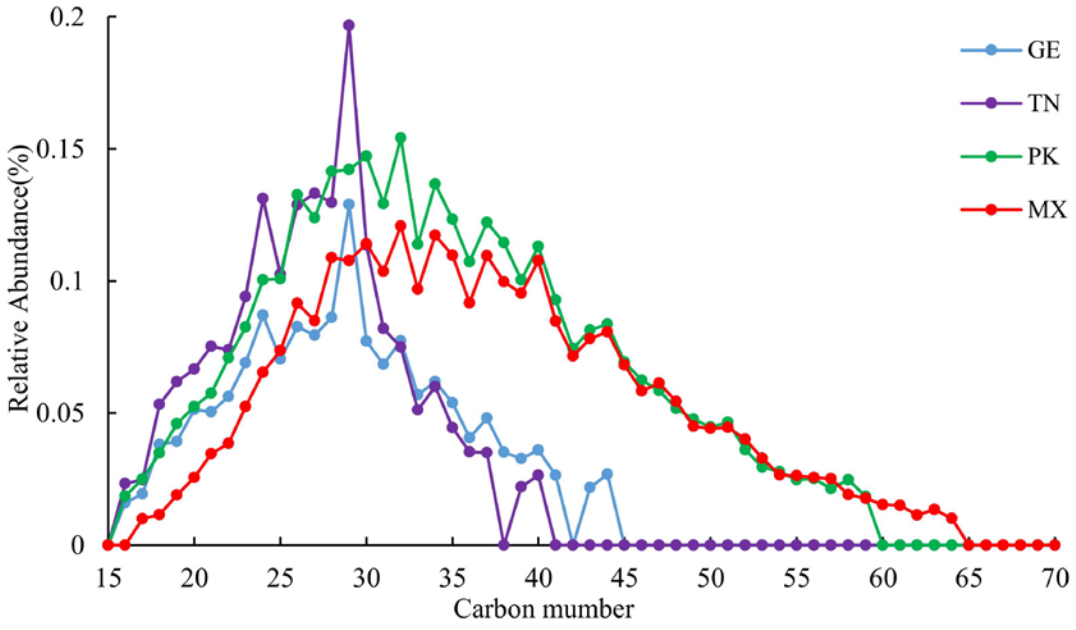

Fig. 9. Carbon number distribution of the double bond equivalence (DBE) 5 groups of the aromatic hydrocarbons of the inclusion oil samples GE, TN, PK and MX. Sample types see Table 1.

915 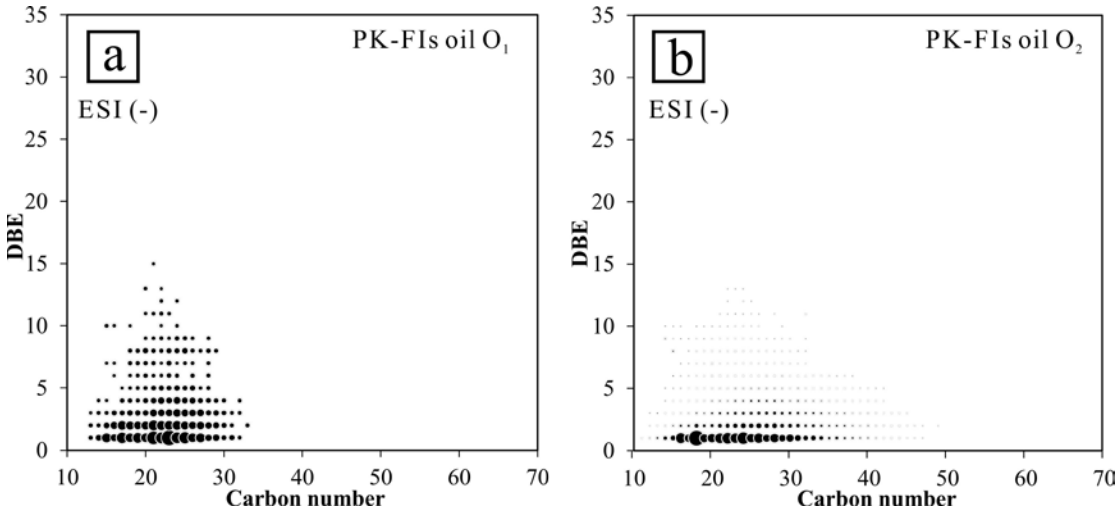

916 Fig. 10. Double bond equivalence (DBE) versus carbon number plots of a) O_1 and b)

917 O_2 compounds in the PK sample measured in ESI (-) mode.

918